Electronic Supplementary Material (ESI) for Journal of Materials Chemistry A.

Single-crystal nickel-rich material as a highly stable cathode for lithium-ion batteries

Aihua Ran [a,b], Shuxiao Chen [a,b], Ming Cheng [a,b], Zheng Liang [a,b], Baohua Li [b], Guangmin Zhou [a,b,], Feiyu Kang [a,b], Xuan Zhang [a,b*], and Guodan Wei [a,b*]*

[a]*Tsinghua-Berkeley Shenzhen Institute (TBSI), Tsinghua University, Shenzhen, 518055, China*

[b]*Tsinghua Shenzhen International Graduate School, Tsinghua University, Shenzhen, 518055, China*

Email contact: guangminzhou@sz.tsinghua.edu.cn; xuanzhang@sz.tsinghua.edu.cn; weiguodan@sz.tsinghua.edu.cn

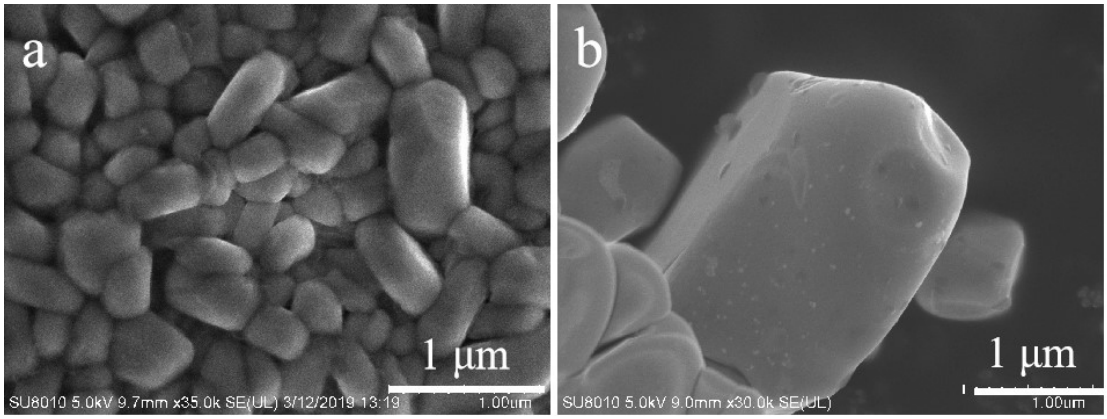

Fig. S1. SEM images of (a) polycrystalline $LiNi_{0.8}Co_{0.1}Mn_{0.1}O_2$ (P-NCM811) and (b) single crystal $LiNi_{0.8}Co_{0.1}Mn_{0.1}O_2$ (S-NCM811).

Sample	a (Å)	c (Å)	V (Å^3)	c/a
P-NCM811	2.874	14.208	101.622	4.944
S-NCM811	2.884	14.246	102.598	4.94

Table S1. Crystal structural parameters of P-NCM811 and S-NCM811.

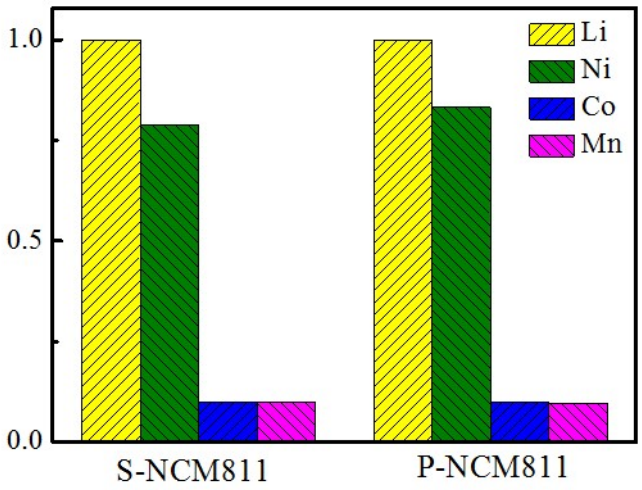

Fig. S2. ICP-OES result for the chemical composition of the two samples.

Fig. S2 displays the chemical composition of NCM, analyzed using ICP-OES (detail value in **Table S2**), which gives the total amount of each element regardless of

its spatial distribution and phase. The proportion of Ni:Co:Mn is close to 8:1:1 for P-NCM811 and S-NCM811.

Sample/Element	Li	Ni	Co	Mn
P-NCM811	1	0.83224	0.09997	0.09729
S-NCM811	1	0.78701	0.09894	0.09736

Table S2. The relative proportion of Li, Ni, Co, and Mn for the P-NCM and S-NCM from the ICP-OES results.

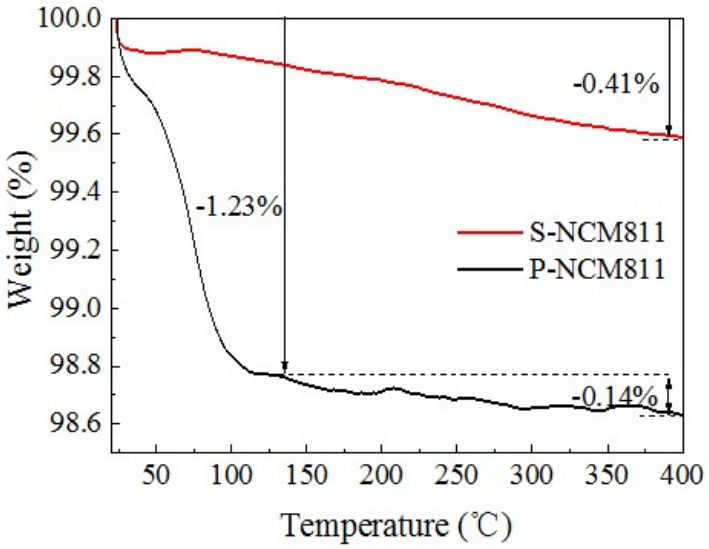

Fig. S3. The thermogravimetric (TG) analyses of P-NCM811 and S-NCM811 cathode between 25℃ and 400℃.

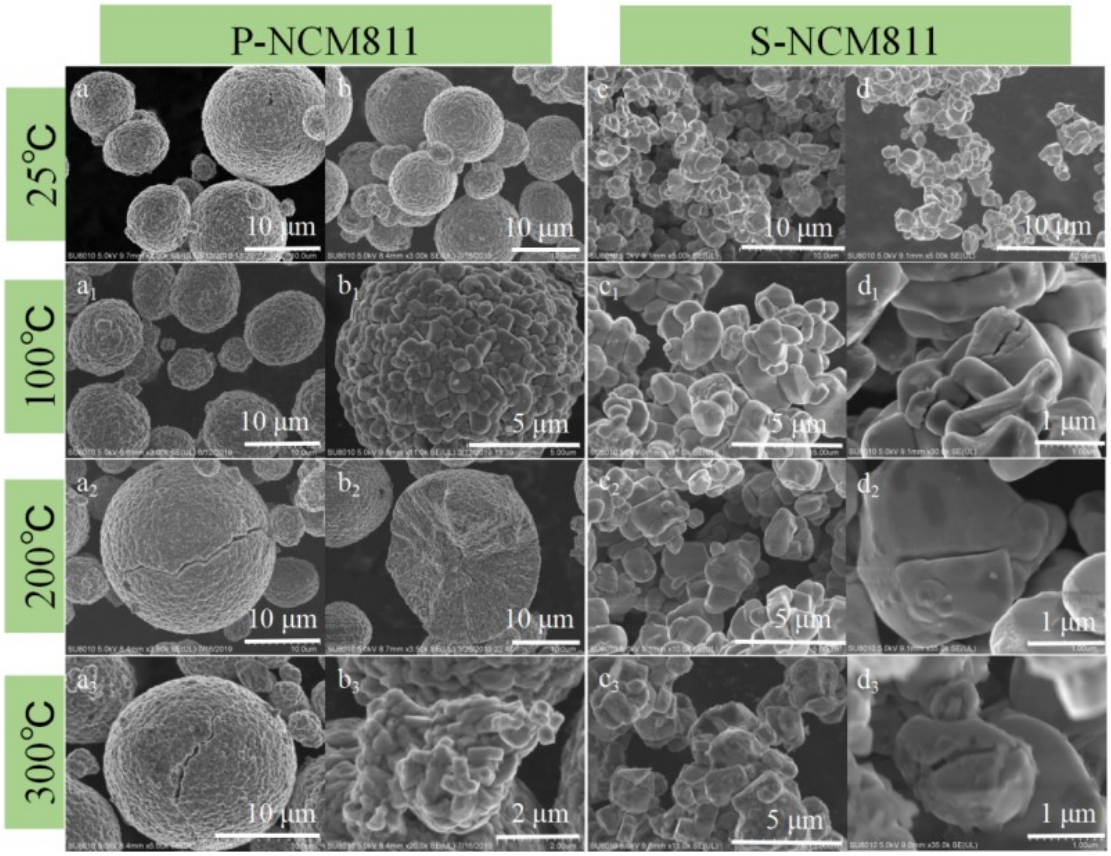

Fig. S4. Morphology changes of P-NCM811 and S-NCM811 after heat treatment at room temperature, 100, 200, and 300 ℃, respectively.

In group a and b, the morphologies of P-NCM811 changed after treatment at different temperatures. Groups c and d represent morphologies of S-NCM treated at different temperatures. As can be seen from the figure, as the temperature increases, the cracks of P-NCM811 increase and the irreversible morphology changes become more serious (a2, a3), and the secondary particles will break into hemispherical particles (b2) or even smaller particles (b3). However, for S-NCM811, with the increase of temperature, single crystal particles will also have cracks, as shown in figure d1 and d2, but it is difficult to find cracks. Therefore, it can be concluded that the high temperature resistance of single crystal particles is better than that of polycrystals.

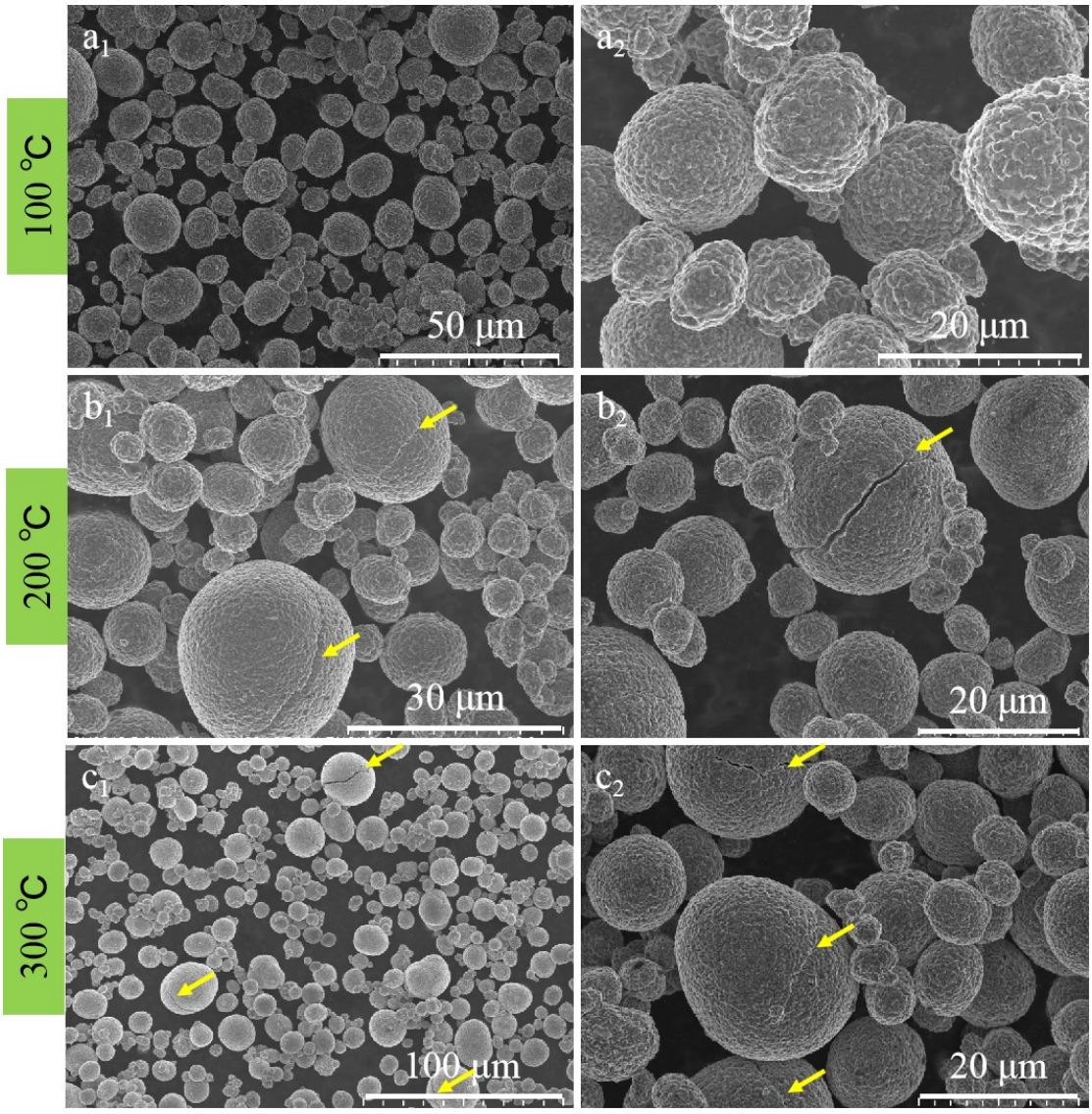

Fig. S5. Morphology changes of P-NCM811 after heat treatment at 100, 200 and 300 ℃, respectively.

As can be seen from Fig. S5a1 and a2, P-NCM structure is maintained well after 100℃ treatment, and no rupture detected. In Fig. S5b1 and b2, the fracture formation of larger particles can be clearly seen. After 300℃ treatment, the degree of rupture is further intensified. For example, cracks can be seen in three particles in Fig. S5c1 and c2. This broader and cracking formation trend further confirms the poor thermal stability of P-NCM811.

	P-NCM811				S-NCM811			
T(℃)	a (Å)	c (Å)	V	c/a	a (Å)	c (Å)	V	c/a
25	2.874	14.208	101.622	4.944	2.884	14.246	102.598	4.940
50	2.875	14.211	101.698	4.944	2.885	14.249	102.719	4.939
75	2.875	14.224	101.790	4.948	2.885	14.252	102.710	4.940
100	2.876	14.226	101.896	4.947	2.885	14.261	102.825	4.942
125	2.877	14.236	102.021	4.949	2.886	14.269	102.937	4.944
150	2.877	14.243	102.084	4.951	2.886	14.278	103.005	4.947
175	2.878	14.259	102.246	4.955	2.888	14.275	103.135	4.942
200	2.878	14.257	102.297	4.953	2.888	14.288	103.194	4.948
225	2.879	14.260	102.385	4.953	2.889	14.297	103.342	4.949
250	2.880	14.270	102.491	4.955	2.889	14.294	103.309	4.948
275	2.881	14.276	102.646	4.954	2.889	14.301	103.372	4.950
300	2.882	14.281	102.747	4.955	2.890	14.311	103.492	4.952
25	2.873	14.219	101.623	4.950	2.884	14.246	102.618	4.940
Change%	0.295	0.513	1.107	0.218	0.204	0.460	0.871	0.255

Table S3. Crystal structural parameters of P-NCM811 and S-NCM811 under *in-situ* XRD test.

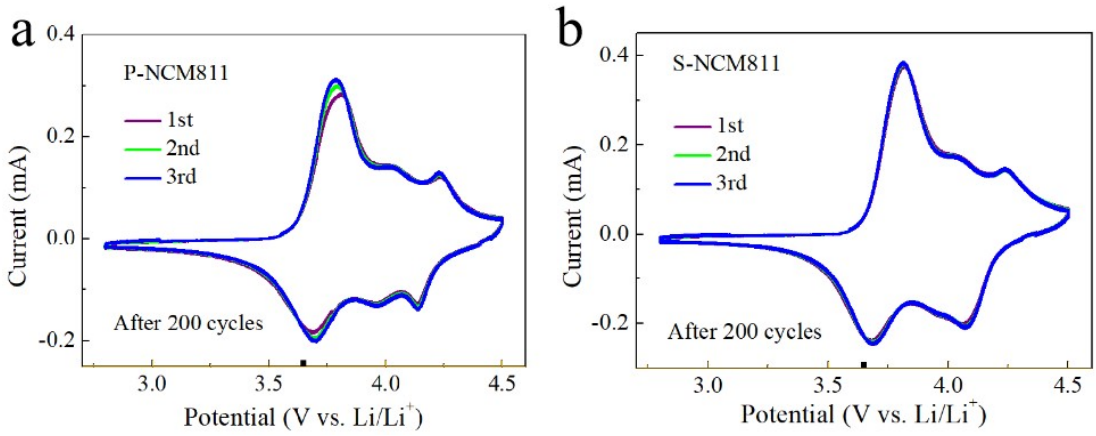

Fig. S6. CV curves of (a) P-NCM811 and (b) S-NCM811 after 200 cycles.

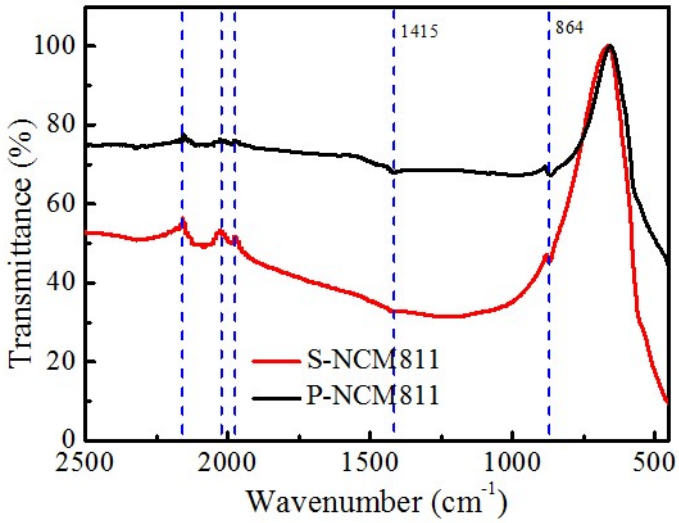

Fig. S7. FTIR spectra of P-NMC811 and S-NCM811.

FT-IR was applied to investigate the surface chemical composition of the two samples as shown in **Fig. S7**.The peak at 530 cm^{-1} represents the metal-oxygen bond (M-O, M=Ni, Co, Mn), which is seen in the two samples. The peaks at 1488 and 1438 cm^{-1} are caused by the antisymmetric stretching vibration of the -CO_3 group and the peak at 868 cm^{-1} is due to the out-of-plane bending vibration of the -CO_3 group. These peak signals indicate that the impurities are composed of carbonate.

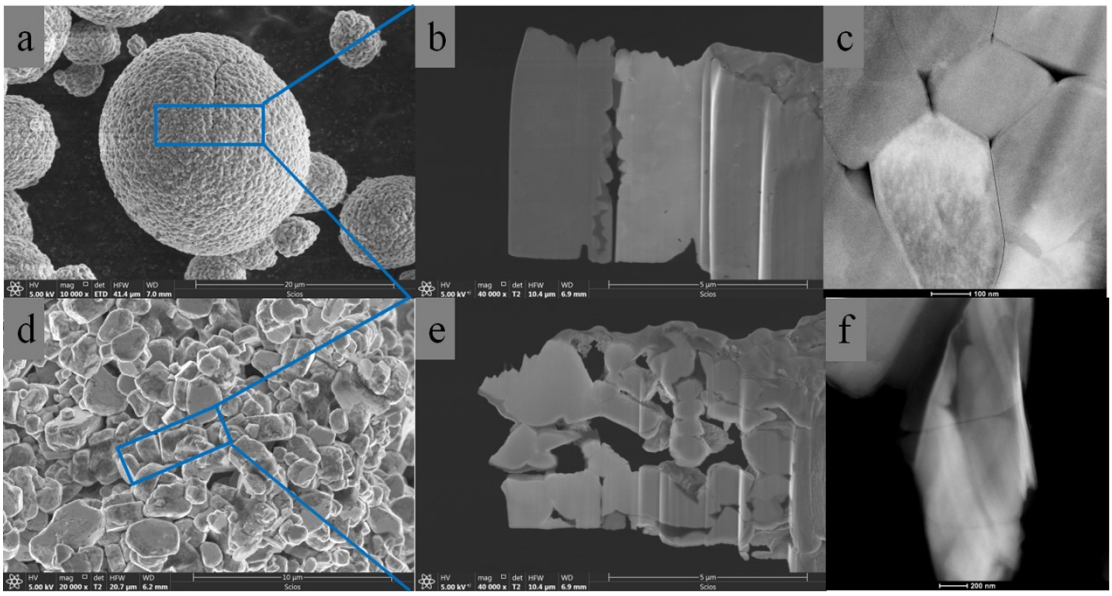

Fig. S8. SEM-FIB images of P-NCM811 (a,b,c) and S-NCM811 (d,e,f).